Applied Physics A (2018) 124:223
https://doi.org/10.1007/s00339-018-1619-0

Applied Physics A
Materials Science & Processing

Properties of Al- and Ga-doped thin zinc oxide films treated with UV laser radiation

Hayder J. Al-Asedy[1,2,3] · Shuruq A. Al-Khafaji[4] · Hazri Bakhtiar[1] · Noriah Bidin[1]

Received: 6 December 2017 / Accepted: 27 January 2018

Abstract
This paper reports the Nd:YAG laser irradiation treated modified properties of aluminum (Al) and gallium (Ga) co-doped zinc oxide (ZnO) (AGZO) films prepared on Si-substrate via combined sol–gel and spin-coating method. The impact of varying laser energy (150–200 mJ) on the structure, morphology, electrical and optical properties of such AGZO films were determined. Laser-treated samples were characterized using various analytical tools. Present techniques could achieve a high-quality polycrystalline films compared with those produced via conventional high temperature processing. AGZO films irradiated with third harmonics UV radiation (355 nm) from Nd:YAG laser source revealed very low resistivity of 4.02×10^{-3} Ω cm. The structural properties grain size was calculated firm the X-ray diffraction spectra using the Scherrer equation that increased from 12.7 to 22.5 nm as the annealing laser energy increased from (150–200) mJ. The differences in crystallinity and orientation are explained in terms of the thermal effect caused by laser irradiation. (FESEM) images have been demonstrated that Nd:YAG laser annealing can significantly improve the crystallinity level, densification, and surface flatness of sol–gel derived AGZO thin films that occurred as a result of laser processing. Synthesized AGZO films displayed favorable growth orientation along (101) lattice direction. AGZO films with energy band gap of 3.37–3.41 eV were obtained. Results on the crystallinity, surface morphology, roughness, bonding vibration, absorption, photoluminescence, and resistivity of the laser-irradiated films were analyzed and discussed.

1 Introduction

In recent times the research on Zinc oxide (ZnO) nanomaterial has been escalating at rapid space due to the feasibility of diverse optoelectronic applications. ZnO is a wide band gap (3.37 eV) n-type semiconductor with distinctive electrical and optical properties. Earlier, ZnO thin films with crystalline orientation along *c*-axis were exploited in surface acoustic wave devices. Lately, ZnO films doped with Al or In have intensively been studied with the aim of achieving transparent conducting electrodes (TCEs) [1–4]. Room temperature prominent luminescence emission from ZnO films became attractive owing to its potential application in UV laser diodes [5, 6] and phosphor for low-voltage flat panel displays [7, 8].

Past researches revealed that the electrical and optical properties of ZnO films are strongly decided by the chemical composition and crystallographic orientations. Generally, non-stoichiometric undoped ZnO films show low electrical resistivity due to oxygen vacancy and zinc interstitials. Besides, high crystallinity and preferred lattice orientation of the undoped ZnO films also contribute to low electrical resistivity [9]. Amongst TCEs, indium tin oxide (ITO) is the dominant one despite several disadvantages such as rareness of Indium, expensive, chemical instability in the reducing ambience, environmental hazards and toxicity to human. To achieve optimal device performance and reduce production cost, alternative electrode materials are opted. Doped or co-doped ZnO film is believed to be a suitable alternative to ITO films. Interestingly, ZnO is an abundant, non-toxic, and chemically stable semiconductor. Hydrogen

✉ Noriah Bidin
noriah@utm.my

[1] Laser Center, Ibnu Sina Institute for Scientific and Industrial Research, University Technology Malaysia, 81310 Johor Bahru, Johor, Malaysia

[2] Department of Physics, Faculty of Science, Universiti Teknologi Malaysia, 81310 Johor Bahru, Johor, Malaysia

[3] Physics Department, Faculty of Education, University of Al-Qadisiyah, Diwaniyah 00964, Iraq

[4] Roads and Transports Department, Faculty of Engineering, University of Al-Qadisiyah, Diwaniyah 00964, Iraq

Published online: 09 February 2018

plasma processes are commonly used for the fabrication of stable ZnO-based solar cells [10, 11].

Currently, few studies hinted that Al-doped ZnO (AZO) material has many advantages in terms of enhanced film conductivity [12] and thermal/chemical stability [13]. Meanwhile, Ga-doped ZnO (GZO) film manifests excellent conductivity and durability against extreme humidity [14–16]. Thus, it seems that co-doping of ZnO with Al and Ga may be beneficial in terms of improved device performance due to modified properties. Very few researches were conducted on Al/Ga co-doped ZnO (AGZO) thin films [17, 18]. It was found that much shorter crystal ionic radius of Al (r_{Al} = 67.5 pm) than Zn (r_{Zn} = 88.0 pm) causes lattice distortion when Zn is substituted by Al in the ZnO lattice, which partly causes the deterioration of electrical conductivity. Though the ionic radius of Ga (r_{Ga} = 76.0 pm) is shorter than Zn, but the degree of their mismatch is much smaller than that of with Al. Some studies exhibited that the optical and electrical properties of AZO film can further be enhanced via the co-doping of Ga. However, most of the existing thin film deposition methods are relied on the expensive and cumbersome vacuum based processing. Kang et al. [17] acknowledged that extra Ga doping into AZO system could led to the relaxation of the induced stress in the film and thereby lower the resistivity because of the minor mismatch of ionic radius of Ga and Al [19]. However, for practical applications further enhancement in the optical and electrical properties became prerequisite.

Over the years, several physical and chemical techniques have been developed to synthesize high-quality two- and three- dimensional (2D and 3D) ZnO nanostructures. These techniques include chemical solution deposition [20], physical vapor deposition [21], catalyst-free processing [22], metal organic chemical vapor deposition [23], thermal evaporation process [24], vapor–liquid–solid method [25], and sol–gel processes [26]. Among all these techniques, sol–gel process offers many advantages for the deposition of thin film. This is due to the excellent control of sol–gel method on the stoichiometry of precursor solution, ease of compositional modifications, homogeneity, cost-effectiveness, film homogeneity on molecular level, low temperature and absence of vacuum [27]. Semiconductor industry exploits pulsed laser ablation to improve various properties of polycrystalline semiconductor films. The effects of laser irradiation on the AZO films were determined [28]. Many researchers studied the influence of excimer laser irradiation on the overall properties of oxide films. For instance, Imai et al. reported the effects of laser treatment on the sol–gel derived indium oxide films [29]. SzoÈreÂnyi et al. examined the impact of laser treatment on the properties of ITO films prepared by dc sputtering [30].

Post-treatment of semiconductor nanostructures via laser irradiation is meritorious in terms of desirable local structural properties improvement by controlling the beam size and positions through masks. Sengupta et al. [31] used single spin-coating deposition and sol–gel method to prepare pure ZnO and Al-doped Zinc Oxide (AZO) thin films on quartz substrate from anhydrous zinc acetate [$Zn(C_2H_3O_2)_2$], monoethanolamine [$H_2NC_2H_4OH$] and isopropanol. Nagase et al. [32] deposited crystalline ZnO films on glass substrates using sol–gel method and post treated the films via KrF excimer laser irradiation. The structures, optical and electrical properties of the laser-irradiated films were analyzed and compared with heat-treated films. Laser irradiation treatment produced two kinds of crystalline ZnO films depending on the energy of laser pulse. At low energy, it produced low crystallinity with weak lattice orientation. Moreover, high irradiation energy achieved high crystallinity with strong lattice orientation. The differences in crystallinity and orientation were explained in terms of laser irradiation assisted thermal effect.

Tsang et al. [28] prepared AZO films using sol–gel spin-coating at low substrate temperature (300 °C) in air and post treated them by KrF excimer laser irradiation (at 200 nm) of altering energies. Overall properties of the laser-irradiated films were analyzed and compared with those prepared by conventional high temperature processing. The laser-irradiated AZO film revealed a low resistivity of 44×10^{-3} Ω-cm and very high optical transmittance (90%) in the visible range. These films were oriented preferentially along (002) lattice direction [28]. Hsiao et al. [33] synthesized TCO thin films with visible transmittance above 80% and high electrical conductivity. These TCO films were targeted for the implementation in flat panel displays and solar cells. They aimed to develop a direct patterning technology on ZnO:Al (AZO) thin films by a diode-pumped solid state (DPSS) UV laser. Hsiao et al. [34] prepared AZO films using DPSS UV laser assisted hybrid process (patterning and annealing). A Nd:YVO_4 UV laser source (355 nm) with peak power of 14 W was used. Regardless of all these approaches an optimized method for AGZO films with desirable properties is far from being attained.

Considering the application prospects of AGZO films, we deposited them on silicon substrates via sol–gel assisted spin-coating method. Prepared AGZO films were post-treated using UV laser irradiation in the ambient air atmosphere. Conventional sol–gel deposition of AZO films requires high temperature (400–500 °C) and prolonged duration for annealing (3 h) which causes the damage of films and substrate due to over-heating. To overcome the high temperature annealing related adverse effects, AGZO samples were post-treated with laser irradiation. The photo-induced influence of selective laser absorption by the overlaying film could modify their overall properties. Besides, laser irradiation (selective excitation) led to rapid crystallization of the precursor films and atomic dissipation from

the film without affecting the substrates, owing to of the films. Laser irradiation assisted electronic excitation could produce defects in the crystals. As-grown AGZO films were characterized using X-ray diffraction (XRD), ellipsometry (Gaertner L166C Ellipsometer to measure the AGZO film thickness grown on Si-substrate), field emission scanning electron microscopy (FESEM), transmission electron microscopy (TEM), energy dispersive X-ray, Fourier transform infrared (FTIR), absorption and photoluminescence (PL) spectroscopy, and four-point probe measurement. The impact of changing laser energy irradiation on the properties of AGZO films was determined.

2 Experimental procedure

2.1 Cleaning of Si-substrate

Al/Ga co-doped ZnO (AGZO) thin films were deposited on p-type Si(100) substrate via sol–gel assisted spin-coating methods. Si-substrate each of dimension (2.5 cm × 2.5 cm) was rinsed with Decon 90 surfactant solution for about 15 min to remove the dust particles from the substrate surface. Next, each substrate was washed with deionized water to eliminate the presence of surface contamination completely that could led to poor adhesion and appearance of pinholes on the deposited film [35]. Afterward, all substrates were oven dried at 150 °C for about 25 min to evaporate entirely the residual water or solvent.

2.2 Preparation of precursor solution

Analytical grade high purity (Alfa Aesar, 99.999%) reagents of zinc acetate dehydrate ($Zn(CH_3COO)_2{\cdot}2H_2O$), aluminum nitrate nonahydrate ($Al(NO_3)_3{\cdot}9H_2O$), gallium nitrate nonahydrate ($Ga(NO_3)_3{\cdot}9H_2O$), 2-propanol and ethanolamine were used to grow the AGZO films. Zinc acetate nonahydrate was first dissolved in a mixture of 2-propanol and ethanolamine at room temperature. The chosen concentration of zinc acetate was 0.1 M and the molar ratio of ethanolamine to zinc acetate was 1:1. The solution was stirred continuously for 30 min using a magnetic stirrer to obtain a homogeneous and transparent clear solution. Each solution with different Ga contents was dissolved in methanol at 60 °C for 90 min and thoroughly stirred to attain a transparent mixture. Then, few drops of the solution were placed on p-type Si(100) substrate and spin-coated at the revolution of 3000 rpm for 30 s. The coating process for each sample was repeated for 10 times to achieve uniform AGZO films. Finally, the obtained AGZO films were further dried at 300 °C for 20 min and annealed using Nd:YAG laser at varying energies to modify the sample properties as described hereunder.

2.3 Laser irradiation treatment on spin-coated AGZO precursor films

After the spin-coating, each sample was baked in a furnace at 300 °C for 15 min to evaporate any organic solvents and impurities present in the coated film. The processes of spin-coating and baking were repeated 10 times until the AGZO film attained a thickness of 240 nm. Then, the film was exposed to Nd:YAG laser irradiation (wavelength of 355 nm) which could heat up the AGZO film while minimizing the substrate heating. The laser beam was exposed directly on the film surface through a window of area 0.1963 cm^2. The number of laser impingements was set to 5 at a frequency of 1 Hz. Laser energy was varied to 150, 160, 170, 180, 190 and 200 mJ corresponding to single shot densities of 763.94, 814.87, 865.80, 916.73, 967.66 and 1018.59 mJ/cm^2, respectively.

Structural analysis of the prepared AGZO films were performed using XRD (Bruker D8 Advance Diffractometer) with Cu–$K\alpha_1$ radiations (1.5406 A°) operated at 40 kV and 100 mA in the scanning angle (2θ) range of 20°–80°. A slow speed of scanning ($\approx 1.2°$/min) with a resolution of 0.01° was used. Samples elemental composition and surface morphology were analyzed using EDX spectroscopy and FESEM (ZEISS SUPRA 35 VP), respectively. Surface morphology of as-grown films was imaged using TEM (Hitachi HT7700). The selected area electron diffraction (SAED) patterns were recorded on a high-resolution TEM (HRTEM, JEOL JEM-ARM200F). Room temperature photoluminescence (PL) spectra were recorded on a Perkin Elmer LS 55 Luminescence Spectrometer, wherein Xenon flash lamp (wavelength of 320 nm) was used as excitation source, and UV–Vis absorption spectra in the wavelength region of 200–800 nm are captured via a PerkinElmer Lambda-25 spectrometer. The electrical resistivity of the annealed AGZO nanofilms was measured using four-point probe method.

3 Results and discussion

3.1 Absorbance spectra

Figure 1 illustrates the absorbance of the spin-coated AGZO film after high temperature (300 °C) baking during sol–gel processing. First, the absorbance of the glass substrate was checked and then for the Si-substrate before treating the spin-coated AGZO films with laser irradiation. In this process, a suitable laser wavelength was chosen to make sure that the AGZO film absorbs the laser energy efficiently. The occurrence of an intense absorption band shown by the AGZO film clearly confirmed the incomplete vaporization and decomposition of ZnAc. Furthermore, the amount of

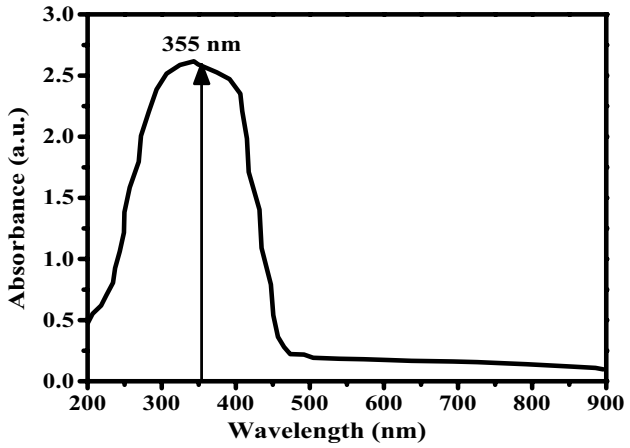

Fig. 1 Absorption spectra of the spin-coated AGZO films after baking at 300 °C

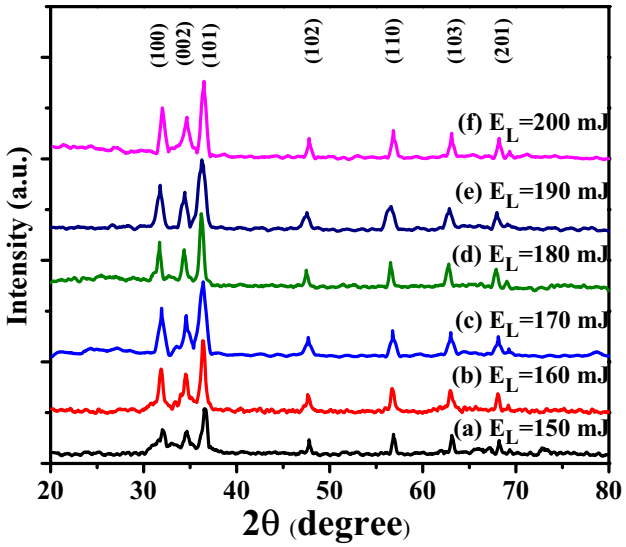

Fig. 2 Influence of laser-irradiation on the XRD patterns of the proposed AGZO films

residual acetate group from the starting material (ZnAc) depended on the drying temperature. Present results were consistent with the report of Nagase et al. [32], wherein two IR absorption bands located at 1580 and 1450–1420 cm^{-1} corresponding to the acetate group were observed for the AGZO film baked at 200 °C. However, only one peak was observed when the film was baked at 300 °C, indicating the complete removal of most of the organic constituents. The absorption of laser radiation by the AGZO films was remarkably enhanced due to baking at high temperature. Moreover, the laser absorption by the deposited AGZO film was not affected by the baking duration. The wavelength (355 nm) of Nd:YAG laser was selectively absorbed by the AGZO films only and not by the substrate, thereby minimized the heating mediated damages of the substrate. It was affirmed that baking temperature of 300 °C was greatly suitable to induce growth of AGZO nanocrystallites in the spin-coated AGZO film.

3.2 Structural properties

Figure 2 displays the XRD pattern of the dried AGZO film annealed with different laser energy. Many reports revealed that most on the organic compounds in the sol–gel grown ZnO films evaporate and decompose after heating to 300 °C [36]. Tsang et al. have showed that 300 °C is suitable to induce crystal growth in the sol–gel synthesized AZO films, where the laser light absorption (248 nm excimer laser) of the films can be enhanced via baking [28]. Irrespective of laser energy, the XRD pattern of all the films revealed sharp Bragg peaks at 2θ values of 31.86°, 34.42°, 36.28°, 47.68°, 56.53°, 62.92° and 67.36° which were allocated to the growth orientations along (100), (002), (101), (102), (110), (103) and (201) lattice planes. It clearly indicated the presence of good polycrystallinity in the film which consisted mainly of hexagonal wurtzite-type of AZO crystals with growth alignment along *c*-axis. This preferential orientation was attributed to the minimization of the surface energy and internal stress [37]. Further XRD analysis of AGZO nanostructures ensured the complete absence of secondary phase such as Al_2O_3, Ga_2O_3, $ZnAl_2O_4$ or $ZnGa_2O_4$. The observed seven diffraction peaks were matched with the JCPDS 36-1451 of ZnO crystal. The most intense XRD peak corresponded to the (101) lattice growth orientation [38]. The crystallite sizes (D) were estimated using the Scherrer formula [39], were the three main diffraction peaks corresponding to (100), (002), and (101) planes were chosen for averaging:

$$D = \frac{K\lambda}{\beta \cos\theta}, \tag{1}$$

where k is the shape factor taken as 0.9, λ is the wavelength of radiation and θ is the peak position.

The average crystallite size of AGZO in the film annealed at 150 mJ of laser energy was 12.71 nm which was further enlarged to 16.86 nm when the laser energy density was increased to 170 mJ. At lower laser energy up to 170 mJ, the AGZO films exhibited relatively low crystallinity and weak crystallographic orientation along the *c*-axis. However, at higher irradiation (above 180 mJ) the emergence of rapid crystallization led to strong orientation along the *c*-axis. At 200 mJ, the crystal size was enlarged to 22.51 nm as enlisted in Table 1.

Figure 3 represents the variation in the lattice constants (c_o) along *c*-axis as a function of different laser energy exposure. The obtained values of c_o were matched with the JCPDS data file. Interestingly, the values of c_o for

Table 1 Laser irradiation energy dependent variation in the lattice constants, *c*/*a*, volume, density and crystal size *D* (nm) for the proposed AGZO films

Laser energy (mJ)	*a* (A°)	*c* (A°)	*c*/*a*	*V* (A°)^3	ρ (g cm^{-3})	*R* (Ω cm)$\times 10^{-3}$	*D* (nm)
150	3.2307	5.2051	1.6111	47.0479	5.7218	5.75	12.71
160	3.2305	5.2042	1.6109	47.0339	5.7235	6.48	14.32
170	3.2301	5.2034	1.6091	47.0151	5.7258	5.47	16.86
180	3.2299	5.2021	1.6106	46.9975	5.7279	4.02	19.08
190	3.2298	5.2015	1.6105	46.9892	5.7289	4.24	20.93
200	3.2295	5.2009	1.6104	46.9750	5.7306	5.03	22.51

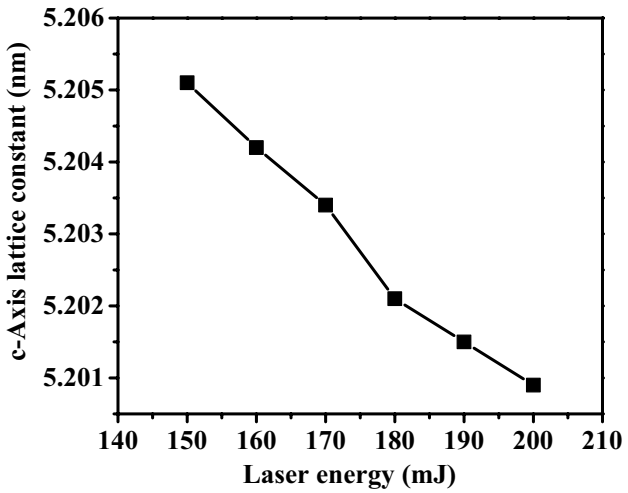

Fig. 3 Laser irradiation energy dependent modification in the *c*-axis lattice constants of AGZO films

laser-irradiated AGZO films were shorter than the heat-treated one. Besides, the lattice constants were shortened steadily with the increase of laser energy. According to Bao et al. [37] report, the values of c_o were slightly higher for ZnO films prepared on quartz glass substrates via sol–gel method followed by heat-treatment. In the present case, the observed lower values of c_o were attributed to the creation of oxygen vacancy, where the presence of such atomic vacancy caused shortening in the lattice constants. Furthermore, the dissipation of oxygen atoms from the ZnO matrix was more viable than the disappearance of Zn atoms. The values of lattice parameters (*a* and *c*) corresponding to the unit cell of hexagonal wurtzite structure was calculated from the main XRD peak following the relation [40]:

$$a = \frac{\lambda}{\sqrt{3}\,\sin\theta_{100}},\ c = \frac{\lambda}{\sin\theta_{002}} \tag{2}$$

Figure 4 depicts the typical EDX spectra of the laser energy (180 mJ) annealed AGZO film. The spectra clearly supported TEM images where the creation of oxygen vacancy was revealed. The EDX results indicated that crystallized laser-irradiated films with lower c_o values produced smaller intensity ratios of O K_α to Zn K_α than the one obtained with heat-treatment. The shortening of c_o values signified an increase in the amount of the resultant oxygen vacancy with increasing laser energy exposure. Furthermore, the intensity of the (101) peak was correlated to the laser energy variation (Fig. 2). It was asserted that the laser irradiation at higher level lead to enhanced crystallization and strong lattice orientation of ZnO phase accompanied by large number of oxygen vacancy creation.

Fig. 4 Typical EDX spectra of AGZO film annealed with laser energy of 180 mJ

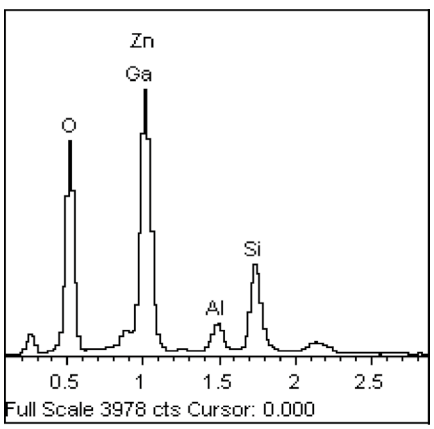

Element	App Conc.	Weight %	Atomic %
O K	0.95	35.01	61.48
Al K	0.01	1.04	1.03
Si K	0.18	14.35	13.76
Zn L	0.52	48.54	22.68
Ga L	0.01	1.06	1.05
Total		100.00	

The value of crystal density (ρ) for the hexagonal AGZO system was calculated from the XRD pattern using the expression:

$$\rho = 1.6609 \times M \frac{n}{a^2 c} \times 0.866, \quad (3)$$

where M is molecular weight of the substance and n is the number of formula units in the unit cell ($n=2$ for ZnO), a and c are the lattice constants of the unit cell [41]. Table 1 enlists the structural properties of the AGZO films as a function of laser energy irradiation.

Values of crystalline density in the film (Table 1) were enhanced with the increase of laser energy irradiation. Generally, thin films enclose point defects, vacancies (cations and anions) and extended defects like dislocations, etc. Presence of these defects was responsible for the augmentation in the density and bulk modulus of the proposed AGZO films. At lower laser energy (150 mJ) these defects were neutralized and did not influence the crystallite size. However, as the energy of laser was increased gradually to 200 mJ the crystallite size and micro-strain depended on the film thickness. The increase in density with the increase in laser energy indicated the volume contraction of the lattice, which further supported by the change in the axial ratio (c/a) of the film.

3.3 FTIR spectra

Figure 5 shows the typical FTIR spectra of four samples irradiated with laser energies in the range of 170–200 mJ. The characteristic functional groups present on the surface of the AGZO films were observed. The spectra clearly revealed that the amount of residual acetate group from the starting material (ZnAc) depended on the drying temperature. Nagase et al. [32], studied sol–gel grown preheated (200 °C) AGZO film and observed two absorption bands (1580 and 1450–1420 cm^{-1}) corresponding to the acetate group, which indicated incomplete vaporization and decomposition of ZnAc in the film. However, in the present work the film baked at 300 °C did not show any such peaks, indicating most of the organic constituents were removed. The formation of AGZO nanocrystallites onto the film surface shown by several FTIR peaks confirmed the impact of laser energy annealing treatment on the crystallinity of the grown AGZO film.

The broad absorption band around 3390–3545 cm^{-1} was assigned to the O–H stretching vibrations [42], which indicated the existence of water molecule in Zn–O lattice absorbed on the surface of AGZO films. The emergence of this band was attributed to the adsorption of some atmospheric water during FTIR measurements [40]. For all samples, the peaks appeared in the range of 2559.9–2642.48 cm^{-1} were allocated to the (C–H) bonding vibration [43]. The observed bands around 1500–1650 cm^{-1} were approved to the absorption of atmospheric CO_2 on the surface of the film [40]. The band around 1100–1290 cm^{-1} corresponded to the (C–C) bonding vibrations [42]. The occurrence of peaks around 951.87, 945.4 cm^{-1} were allotted to the Si–O bonding vibration aroused from the oxygen passivation on the Si-substrate [44]. The observation of intense absorption bands in the wavenumber range of 890–700, 757.97, 752.94, 769.17 and 769 cm^{-1} were not reported elsewhere. The absorption band around 827.3 cm^{-1} with weak intensity (for AGZO film annealed at 180 mJ) was originated from the overlapping of Zn–O or O–Al–O bonding vibrations [44]. The evidenced broad band centered around 570 cm^{-1} (for AGZO film annealed above 180 mJ of energy) was assigned to the stretching of Al–O bond or aluminum oxide lattice [45]. Commercial bulk ZnO powders show absorption band around 442.6 cm^{-1}, whereas the main absorption band of AGZO film was shifted to 448.1, 416.04, 428.88 and 438.5 cm^{-1}. These IR bands shift at laser annealing energy above 170 mJ with decreasing in the intensity (increased aluminum content) accompanied by broadening indicated the vacancies assisted structural disorder and poor crystallization of the AGZO films [46].

3.4 Morphological characteristics

Figure 6a–f shows the FESEM images (top view) of grown AGZO thin films at varying laser energy. The crystallite size was increased from 12.71 to 22.51 nm when the laser energy was increased from 150 to 200 mJ. The laser irradiation mediated modifications in the samples crystallinity was majorly attributed to thermal energy absorption by the AGZO films. In short, the AGZO surface morphology was significantly affected by the increasing energy of laser irradiation.

At low laser energy (150 mJ) the surface of the AGZO films revealed dispersion of featureless nanosized particles (Fig. 6a) and some nanovoids [47]. However, as the laser energy was increased to 160 mJ, two types of nanostructures (Fig. 6b) comprising of nanoparticles and nanocircles without any crack was appeared. At slightly higher laser energy (170 mJ) the film surface manifested clear grain boundaries with small grains randomly distributed on the entire film surface (Fig. 6c). At energy of 180 mJ, the emergence of few dark lines along the grain boundaries (Fig. 6d) indicated the development of nanocracks [38]. The formation of inter-granular nanocracks was ascribed to the local non-uniform tensile stress induced by the rapid cooling of the film after irradiation at higher laser energy. It was suggested that by combining the direct printing technique of material solutions with the excimer laser annealing process the magnitude of non-uniform tensile stress can be remarkably reduced,

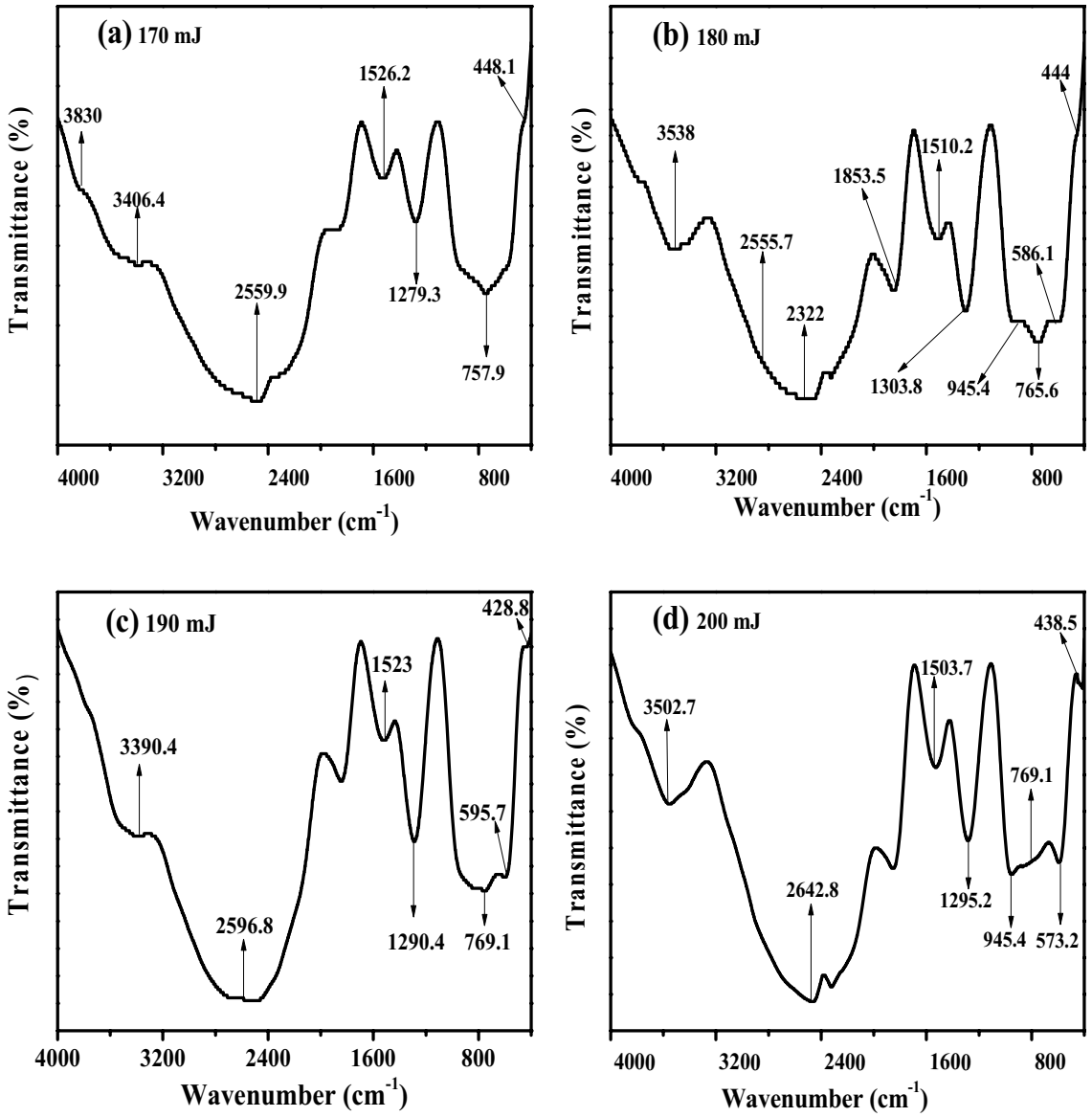

Fig. 5 FTIR spectra of the AGZO films irradiated with laser energy of: **a** 170 mJ, **b** 180 mJ, **c** 190 mJ and **e** 200 mJ

leading to the development of crack-free ZnO thin films. The grain boundaries with larger abnormal grains became more prominent at laser energy of 190 mJ (Fig. 6e) than at lower energies [38]. Finally, at highest laser energy of 200 mJ the FESEM images displayed unique surface morphology where big size AGZO crystallites were evidenced accompanied by enhanced surface roughness (Fig. 6f). At this energy, the film disclosed several broken shaped particles, larger grains, big voids, and greatly rough surface with enhanced damages. This may be related to the direct photo-induced activation of the atoms which could occupy the correct crystal lattice sites due to the availability of laser irradiation assisted enough thermal energy. Consequently, the grains with lower surface energy became larger and the growth orientation becomes stronger, thus leading to an improvement in the crystallinity of AGZO films.

3.5 Photoluminescence spectra

Figure 7 displays the room temperature PL emission spectra of the proposed AGZO films (in the range of 360–400 nm under excitation wavelength of 320 nm) as a function of different energy laser of irradiation. The PL spectra of AGZO films at lower laser energy (170 and 180 mJ) revealed a single broad emission peak around 367.5 nm. However, the PL spectra showed to broad peaks centered at 367.5 nm (intense UV peak) and 450 nm (blue

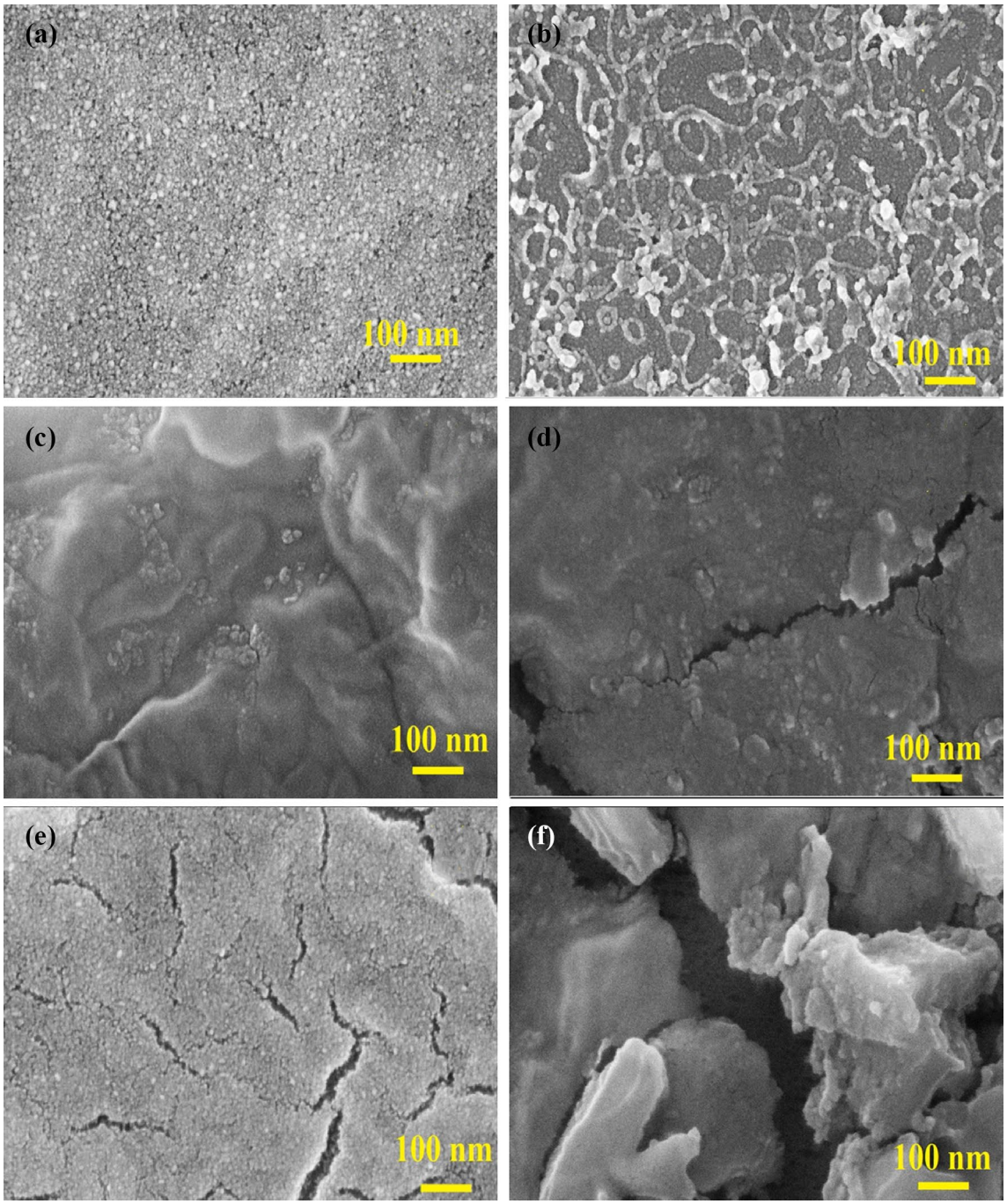

Fig. 6 FESEM images of the AGZO films irradiated with laser energy of: **a** 150 mJ, **b** 160 mJ, **c** 170 mJ, **d** 180 mJ, **e** 190 mJ, and **f** 200 mJ

visible weak). The intense PL peak situated at 367.5 nm revealed a blue shift as the laser energy was increased from 170 to 200 mJ. This observed blue shift was attributed to the shallow binding of the excitons that were formed during high temperature annealing [40]. Meanwhile, the weak PL peak positioned at 450 nm revealed a red shift as the laser energy was increased from 190 to 200 mJ.

The violet emission peak was attributed to the electronic transition from defect level, corresponding to high concentration zinc interstitials to the valence band. It has been reported that stoichiometric pure ZnO thin films usually show strong UV luminescence and no visible spectrum. However, the presence of any visible luminescence in the spectrum can be ascribed to the defects mediated deep level

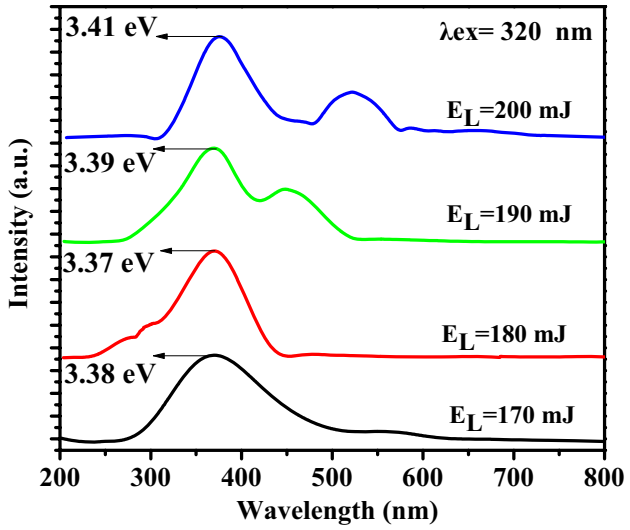

Fig. 7 PL spectra for AGZO films treated with laser irradiation of varying energy

emissions such as Zn interstitials or oxygen vacancies [48]. In the present work, complete absence of any visible luminescence indicated the purity and stoichiometric perfection of the prepared AGZO films. The broad and intense emission peak around 365 nm was attributed to the excitonic transition. The occurrence of blue peak at around 450 nm (at lear enegy of 190 mJ) was related to Zn vacancy (V_{Zn}) as an acceptor [49]. The intensity of the blue peak was changed accompanied by a shift (at laser energy of 200 mJ). The appearance of a second visible green peak of low intensity around 530 nm was attributed to the presence of photo-excited holes, singly ionized oxygen vacancies (V_O) [7] and oxygen antisite (O_{Zn}) in the AGZO films [50]. Although the origin of the green peak remained debatable, but currently there is a general consensus that the UV emission of ZnO is related to the exciton recombination via an exciton–exciton collision process. Meanwhile, the mechanism of the blue-green emission can be related to the oxygen vacancy or Zn interstitials [51]. Vanheusden et al. [7] explained the blue-green emission as a recombination of a photo-excited hole and the singly ionized-charge oxygen vacancy.

3.6 HRTEM images

Figure 8a displays the HRTEM image of the AGZO film irradiated with laser energy of 180 mJ. Figure 8b clearly resolved the corresponding single lattice fringes with inter-plane distance of 0.2474 nm (the distance between two fringes), which matched with the (101) lattice plane at angular position of 36° occurred in the XRD pattern [52]. The HRTEM images clearly revealed the nature of polycrystalline film with multilayer growth pattern consisting of NPs and the presence of round-shaped crystallites with distinct crystallographic planes. Interesting enough, post-treatment of the the AGZO film using laser irradiation at varying energies could achieve high regularity in the fringe profile. This in turn confirmed the attainment of good quality, homogeneity and enhanced crystallinity of the nanostructured AGZO thin film [52].

Several researchers have been studied the overall properties (morphological, electrical and optical) of deposited ZnO on glass as well as silicon substrates and compared them. The mean roughness was found to decrease significantly. It was reported by Ngom et al. [53] and Taabouche et al.

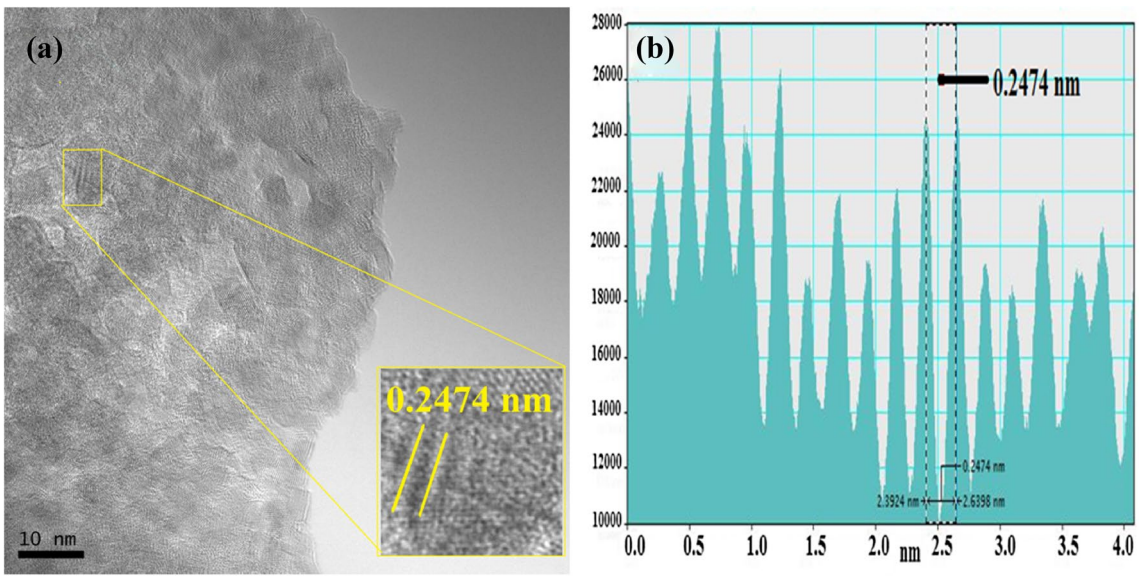

Fig. 8 **a** HRTEM image of AGZO film annealed at laser energy of 180 mJ and **b** the corresponding lattice fringe profile

[54] that an increase in the surface roughness of the films could cause deterioration in the electrical and optical properties. Furthermore, these differences in the mean roughness revealed considerable influence on the optical properties of the films. These results clearly indicated that the film's crystallinity was affected by the nature of substrates and agreed well with the findings of Li et al. [55]. In this work, the AGZO films grown on glass substrate were discerned to be more effective than the one obtained on Si-substrate.

3.7 Resistivity of AGZO films

The electrical resistivity of the laser irradiation treated AGZO films was measured by the four-point probe method. The resistivity of laser-irradiated AGZO films was found to decrease with the increase the laser energy as shown in Fig. 9. At lower energy (below 180 mJ), the observed reduction in the resistivity of the AGZO film was attributed to the enhanced carrier concentration caused by the laser-activated Al ion and lowering in the oxygen vacancies [56]. For laser energy above 180 mJ, the resistivity of AGZO films was increased with the increase of laser energy, which was majorly ascribed to the decrease of carriers' mobility. The increase in the resistivity with increasing laser energy can be related to the raise of films surface temperature. Kim et al. [57] reported the conversion of an ultra-wide band gap amorphous oxide insulator to a semiconductor (Fig. 1b) wherein the electrical conductivity was increased exponentially with the increase in the film density. Our results indeed supported this observation. It was also asserted that good transparent conducting oxides such as Al-doped ZnO (ZnO:Al) could possess high concentration of free electrons ($N_e > 1020\ cm^{-3}$). These

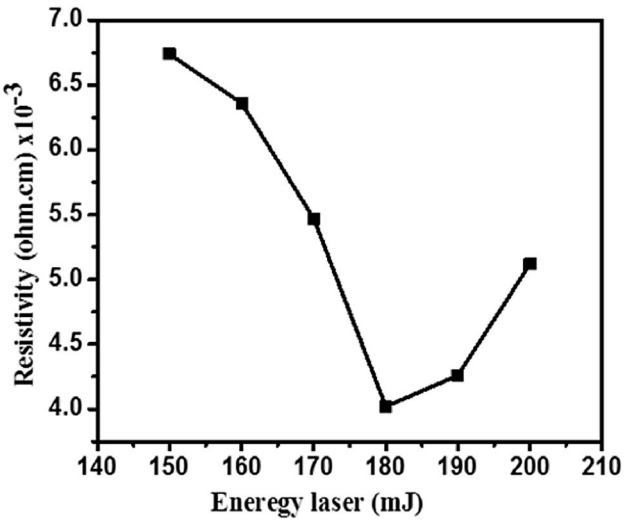

Fig. 9 Laser irradiation energy dependent resistivity of the synthesized AGZO films

electrons were generated from a shallow donor level of Al_{Zn}, wherein the electron trap density (D_t) was negligible compared to the free electron concentration. The blue region in Fig. 4b revealed high density electron traps and/or low-density free electrons generated from the donors, which led to transform the AGZO film to an electrical insulators. Moreover, it is difficult to transform ultra-wide band gap amorphous materials to electronic conductors because of fairly low N_e and high D_t in the former one. Actually, the existence of very deep (at 0.68 eV) donor level (Fig. 4a) in amorphous (a)-Ga_2O_x is responsible for too low N_e ($\approx 10^{15}\ cm^{-3}$) and very high $D_t > 10^{15}\ cm^{-3}$. In the present case, the semiconducting a-Ga_2O_x films were obtained by suppressing D_t as indicated by 'Route (ii)'. Conversely, the increase in the grain size of the annealed AGZO films and the separation between the two neighboring grain boundaries caused lower resistivity, which is consistent with other report [56].

4 Conclusion

We determined the effects of post-laser irradiation treatment on the overall properties of transparent and conductive AGZO films. Such films were prepared on Si-substrate via combined sol–gel and spin-coating technique. The structure, morphology, electrical and optical properties of the Nd:YAG laser irradiation treated AGZO films were significantly improved. Good quality, highly polycrystalline and *c*-axis oriented nanocrystalline AGZO films were achieved. The resistivity of the laser-irradiated film (at 180 mJ) was very low $\approx 4.02 \times 10^{-3}\ \Omega$ cm. The crystallinity of the films was improved with the increase of laser energy, wherein the crystallites revealed strong orientation along (101) lattice plane. Irrespective of laser annealing energy, all AGZO thin films displayed the hexagonal wurtzite structure with strong growth orientation along the (101) plane. However, the highest laser irradiation energy density of 200 mJ induced abnormal grain growth in the films. The long-term goal of this work is to produce selective crystallinity in ZnO using the sol–gel route at the lowest possible thermal damage over small local area via fast annealing. It was demonstrated that Nd:YAG laser irradiation treated sol–gel derived AGZO films with unique structural, morphological, optical and electrical properties are prospective for sundry applications. Our method of AGZO films synthesis may constitute a basis without requirement of special vacuum equipment and high temperature processing as needed by the conventional techniques. It is established that the proposed method can successfully pattern and anneal AGZO films or fabricate other diverse transparent conductive oxide films with desirable properties potential for applications.

Acknowledgements The authors are grateful to the Malaysian Government for providing the financial support through FRGS vote 4F815 in this project. Thanks to RMC and UTM for monitoring the research progress and fund managements and the performance of the project. Thanks are also extended to the Higher Education and Scientific Research, University of Al-Qadisiyah, Faculty of Education, Physics Department of Iraq, for providing PhD study leave.

References

1. S.Y. Myong, S.J. Baik, C.H. Lee, W.Y. Cho, K.S. Lim, Extremely transparent and conductive ZnO:Al thin films prepared by photo-assisted metalorganic chemical vapor deposition (photo-MOCVD) using AlCl3 ($6H_2O$) as new doping material. Jpn. J. Appl. Phys. **36**(8B), L1078 (1997)
2. M.N. Islam, T. Ghosh, K. Chopra, H. Acharya, XPS and X-ray diffraction studies of aluminum-doped zinc oxide transparent conducting films. Thin Solid Films **280**(1), 20–25 (1996)
3. Y. Ohya, H. Saiki, T. Tanaka, Y. Takahashi, Microstructure of TiO_2 and ZnO films fabricated by the sol–gel method. J. Am. Ceram. Soc. **79**(4), 825–830 (1996)
4. Y. Ohya, H. Saiki, Y. Takahashi, Preparation of transparent, electrically conducting ZnO film from zinc acetate and alkoxide. J. Mater. Sci. **29**(15), 4099–4103 (1994)
5. Y. Segawa, A. Ohtomo, M. Kawasaki, H. Koinuma, Z. Tang, P. Yu, G. Wong, Growth of ZnO thin film by laser MBE: lasing of exciton at room temperature. physica status solidi (b). **202**(2), 669–672 (1997)
6. P. Zu, Z. Tang, G.K. Wong, M. Kawasaki, A. Ohtomo, H. Koinuma, Y. Segawa, Ultraviolet spontaneous and stimulated emissions from ZnO microcrystallite thin films at room temperature. Solid State Commun. **103**(8), 459–463 (1997)
7. K. Vanheusden, W. Warren, C. Seager, D. Tallant, J. Voigt, B. Gnade, Mechanisms behind green photoluminescence in ZnO phosphor powders. J. Appl. Phys. **79**(10), 7983–7990 (1996)
8. K. Vanheusden, C. Seager, W. Warren, D. Tallant, J. Caruso, M. Hampden-Smith, T. Kodas, Green photoluminescence efficiency and free-carrier density in ZnO phosphor powders prepared by spray pyrolysis. J. Lumin. **75**(1), 11–16 (1997)
9. D. Bao, H. Gu, A. Kuang, Sol–gel-derived c-axis oriented ZnO thin films. Thin solid films. **312**(1), 37–39 (1998)
10. X. Jiang, F. Wong, M. Fung, S. Lee, Aluminum-doped zinc oxide films as transparent conductive electrode for organic light-emitting devices. Appl. Phys. Lett. **83**(9), 1875–1877 (2003)
11. N. Giebink, Y. Sun, S. Forrest, Transient analysis of triplet exciton dynamics in amorphous organic semiconductor thin films. Org. Electron. **7**(5), 375–386 (2006)
12. H. Kim, A. Pique, J. Horwitz, H. Murata, Z. Kafafi, C. Gilmore, D. Chrisey, Effect of aluminum doping on zinc oxide thin films grown by pulsed laser deposition for organic light-emitting devices. Thin Solid Films. **377**, 798–802 (2000)
13. W. Lee, S. Shin, D.-R. Jung, J. Kim, C. Nahm, T. Moon, B. Park, Investigation of electronic and optical properties in Al–Ga codoped ZnO thin films. Curr. Appl. Phys. **12**(3), 628–631 (2012)
14. T. Minami, Transparent conducting oxide semiconductors for transparent electrodes. Semicond. Sci. Technol. **20**(4), S35 (2005)
15. T. Minami, Substitution of transparent conducting oxide thin films for indium tin oxide transparent electrode applications. Thin Solid Films. **516**(7), 1314–1321 (2008)
16. T. Minami, K. Okada, T. Miyata, J. Nomoto, Y. Hara, H. Abe, Transparent conducting impurity-doped ZnO thin films prepared using oxide targets sintered by millimeter-wave heating. J. Vac. Sci. Technol. A. **27**(4), 1006–1011 (2009)
17. D.-W. Kang, S.-J. Kim, T.-H. Moon, H.-M. Lee, M.-K. Han, Effect of Ga doping on transparent and conductive Al-doped ZnO films prepared using magnetron cosputtering. Jpn. J. Appl. Phys. **49**(12R), 125801 (2010)
18. J.-P. Kim, J.-S. Bae, T.-E. Hong, M.-S. Won, J.-H. Yoon, B.-S. Lee, H.-J. Lee, Optical and electrical properties of ZnO films, codoped with Al and Ga deposited at room temperature by an RF sputtering method. Thin Solid Films. **518**(22), 6179–6183 (2010)
19. M. Park, S.M. Han, Enhancement in conductivity through Ga, Al dual doping of ZnO nanofibers. Thin Solid Films. **590**, 307–310 (2015)
20. O. Lupan, L. Chow, S. Shishiyanu, E. Monaico, T. Shishiyanu, V. Şontea, B.R. Cuenya, A. Naitabdi, S. Park, A. Schulte, Nanostructured zinc oxide films synthesized by successive chemical solution deposition for gas sensor applications. Mater. Res. Bull. **44**(1), 63–69 (2009)
21. G. Jimenez-Cadena, E. Comini, M. Ferroni, A. Vomiero, G. Sberveglieri, Synthesis of different ZnO nanostructures by modified PVD process and potential use for dye-sensitized solar cells. Mater. Chem. Phys. **124**(1), 694–698 (2010)
22. J.-J. Wu, S.-C. Liu, Catalyst-free growth and characterization of ZnO nanorods. J. Phys. Chem. B. **106**(37), 9546–9551 (2002)
23. W.I. Park, D.H. Kim, S.-W. Jung, G.-C. Yi, Metalorganic vapor-phase epitaxial growth of vertically well-aligned ZnO nanorods. Appl. Phys. Lett. **80**(22), 4232–4234 (2002)
24. J. Zheng, Q. Jiang, J. Lian, Synthesis and optical properties of flower-like ZnO nanorods by thermal evaporation method. Appl. Surf. Sci. **257**(11), 5083–5087 (2011)
25. A.D. Chandra, K. Debdulal, S. Fouran, A.D. Kumar, G. Pellegrini, C. Ramesh, M. Paolo, Synthesis of ZnO nanostructures using different metal catalyst: morphology and photoluminescence characteristics. J. Nanosci. Nanotechnol. **10**(4), 2933–2937 (2010)
26. J. Lee, A. Easteal, U. Pal, D. Bhattacharyya, Evolution of ZnO nanostructures in sol–gel synthesis. Curr. Appl. Phys. **9**(4), 792–796 (2009)
27. J. Chatelon, C. Terrier, E. Bernstein, R. Berjoan, J. Roger, Morphology of SnO 2 thin films obtaibed by the sol–gel technique. Thin Solid Films **247**(2), 162–168 (1994)
28. W.M. Tsang, F.L. Wong, M.K. Fung, J. Chang, C.S. Lee, S.T. Lee, Transparent conducting aluminum-doped zinc oxide thin film prepared by sol–gel process followed by laser irradiation treatment. Thin Solid Films **517**(2), 891–895 (2008)
29. H. Imai, A. Tominaga, H. Hirashima, M. Toki, M. Aizawa, Ultraviolet-laser-induced crystallization of sol–gel derived indium oxide films. J. Sol Gel Sci. Technol. **13**(1), 991–994 (1998)
30. T. Szörényi, L. Laude, I. Bertoti, Z. Kantor, Z. Geretovszky, Excimer laser processing of indium-tin-oxide films: an optical investigation. J. Appl. Phys. **78**(10), 6211–6219 (1995)
31. J. Sengupta, R. Sahoo, C. Mukherjee, Effect of annealing on the structural, topographical and optical properties of sol–gel derived ZnO and AZO thin films. Mater. Lett. **83**, 84–87 (2012)
32. T. Nagase, T. Ooie, J. Sakakibara, A novel approach to prepare zinc oxide films: excimer laser irradiation of sol–gel derived precursor films. Thin Solid Films **357**(2), 151–158 (1999)
33. W.-T. Hsiao, S.-F. Tseng, C.-H. Kuo, K.-C. Huang, D. Chiang, P.-C. Yao, M.-F. Chen, Fabrication of electrodes on the aluminum doped zinc oxide thin films using an ultraviolet laser direct-patterning technology. Phys. Proc. **19**, 456–465 (2011)
34. W.-T. Hsiao, S.-F. Tseng, K.-C. Huang, D. Chiang, Electrode patterning and annealing processes of aluminum-doped zinc oxide thin films using a UV laser system. Opt. Lasers Eng. **51**(1), 15–22 (2013)
35. S.A. Van Slyke, C. Chen, C.W. Tang, Organic electroluminescent devices with improved stability. Appl. Phys. Lett. **69**(15), 2160–2162 (1996)

36. H.-C. Cheng, C.-F. Chen, C.-Y. Tsay, J.-P. Leu, High oriented ZnO films by sol–gel and chemical bath deposition combination method. J. Alloy. Compd. **475**(1), L46–L49 (2009)
37. D. Bao, H. Gu, A. Kuang, Sol–gel-derived c-axis oriented ZnO thin films. Thin solid films **312**(1–2), 37–39 (1998)
38. C.-Y. Tsay, M.-C. Wang, Structural and optical studies on sol–gel derived ZnO thin films by excimer laser annealing. Ceram. Int. **39**(1), 469–474 (2013)
39. V. Kumar, R. Singh, N. Singh, A. Kapoor, R. Mehra, L. Purohit, Synthesis and characterization of aluminum–boron co-doped ZnO nanostructures. Mater. Res. Bull. **48**(2), 362–366 (2013)
40. M. Gondal, Q. Drmosh, Z. Yamani, T. Saleh, Synthesis of ZnO 2 nanoparticles by laser ablation in liquid and their annealing transformation into ZnO nanoparticles. Appl. Surf. Sci. **256**(1), 298–304 (2009)
41. D. Behera, B. Acharya, Nano-star formation in Al-doped ZnO thin film deposited by dip-dry method and its characterization using atomic force microscopy, electron probe microscopy, photoluminescence and laser Raman spectroscopy. J. lumin. **128**(10), 1577–1586 (2008)
42. N. Avci, P.F. Smet, J. Lauwaert, H. Vrielinck, D. Poelman, Optical and structural properties of aluminium oxide thin films prepared by a non-aqueous sol–gel technique. J. Sol Gel Sci. Technol. **59**(2), 327–333 (2011)
43. N. Ozer, J.P. Cronin, Y.-J. Yao, A.P. Tomsia, Optical properties of sol–gel deposited Al_2O_3 films. Sol. Energy Mater. Sol. Cells. **59**(4), 355–366 (1999)
44. T. Ivanova, A. Harizanova, T. Koutzarova, B. Vertruyen, Optical characterization of sol–gel ZnO:Al thin films. Superlattices Microstruct. **85**, 101–111 (2015)
45. K. Murali, P. Thirumoorthy, Characteristics of sol–gel deposited alumina films. J. Alloy. Compd. **500**(1), 93–95 (2010)
46. X. Wang, B. Dong, M. Lei, Infrared absorption spectra of Er 3+-doped Al_2O_3 nanopowders by the sol–gel method. J. Sol Gel Sci. Technol. **39**(3), 307–311 (2006)
47. Q. Xu, R. Hong, H. Huang, Z. Zhang, M. Zhang, X. Chen, Z.Y. Wu, Laser annealing effect on optical and electrical properties of Al doped ZnO films. Opt. Laser Technol. **45**, 513–517 (2013)
48. C. Pan, C. Tu, C. Tun, C. Lee, G. Chi, Structural and optical properties of ZnO epilayers grown by plasma-assisted molecular beam epitaxy on GaN/sapphire (0001). J. Cryst Growth **305**(1), 133–136 (2007)
49. X. Wei, B. Man, M. Liu, C. Xue, H. Zhuang, C. Yang, Blue luminescent centers and microstructural evaluation by XPS and Raman in ZnO thin films annealed in vacuum, N_2 and O_2. Phys. B **388**(1), 145–152 (2007)
50. Z. Lei, J.-S. Lian, Y.-H. Liu, Q. Jiang, Influence of preparation methods on photoluminescence properties of ZnO films on quartz glass. Trans. Nonferr. Met. Soc. China. **18**(1), 145–149 (2008)
51. W. Cheng, P. Wu, X. Zou, T. Xiao, Study on synthesis and blue emission mechanism of ZnO tetrapod like nanostructures. J. Appl. Phys. **100**(5), 054311 (2006)
52. S. Baruah, J. Dutta, Hydrothermal growth of ZnO nanostructures. Sci. Technol. Adv. Mater. **10**(1), 013001 (2009)
53. B. Ngom, T. Mpahane, N. Manyala, O. Nemraoui, U. Buttner, J. Kana, A. Fasasi, M. Maaza, A. Beye, Structural and optical properties of nano-structured tungsten-doped ZnO thin films grown by pulsed laser deposition. Appl. Surf. Sci. **255**(7), 4153–4158 (2009)
54. A. Taabouche, A. Bouabellou, F. Kermiche, F. Hanini, S. Menakh, Y. Bouachiba, T. Kerdja, C. Benazzouz, M. Bouafia, S. Amara, Effect of substrates on the properties of ZnO thin films grown by pulsed laser deposition. Adv. Mater. Phys. Chem. **3**(04), 209 (2013)
55. C. Li, M. Furuta, T. Matsuda, T. Hiramatsu, H. Furuta, T. Hirao, Effects of substrate on the structural, electrical and optical properties of Al-doped ZnO films prepared by radio frequency magnetron sputtering. Thin Solid Films **517**(11), 3265–3268 (2009)
56. W. Wang, C. Li, J. Zhang, X. Diao, Effects of atomic oxygen treatment on structures, morphologies and electrical properties of ZnO:Al films. Appl. Surf. Sci. **256**(14), 4527–4532 (2010)
57. J. Kim, T. Sekiya, N. Miyokawa, N. Watanabe, K. Kimoto, K. Ide, Y. Toda, S. Ueda, N. Ohashi, H. Hiramatsu, Conversion of an ultra-wide bandgap amorphous oxide insulator to a semiconductor. NPG Asia Mater. **9**(3), e359 (2017)